Progress In Electromagnetics Research M, Vol. 56, 111–120, 2017

DOA Estimation of Partially Polarized Signals

Minjie Wu*, Tianzhen Meng, and Naichang Yuan

Abstract—In this correspondence, the two-dimensional (2-D) direction-of-arrival (DOA) estimation problem for partially polarized (PP) signals is considered. In particular, we focus on an array geometry containing three identical uniform linear arrays (ULAs). Compared with existing methods, the proposed one has three main advantages. Firstly, the estimation accuracy is higher since it exploits the polarization information. Secondly, it can work effectively under the coexistence of both noncircular and circular signals. Finally, pair matching for 2-D DOA is not required which reduces the computational complexity. Simulation results are presented verifying the efficacy of the algorithm.

1. INTRODUCTION

In the wake of developments in signal processing technology, it is more realistic that the impinging signals to the array are mixed noncircular and circular ones. Considerable alternatives have been presented to cope with this case, e.g., [1–3]. One typical method has been discussed in [2], where all the signals are completely polarized (CP). For CP source, the end point of the electric field traces out an ellipse whose orientation and axial ratio are constant. However, the polarization state of a partially polarized (PP) source is a function of time. In previous literature [4, 5], the incident waves were always assumed to be CP. As a matter of fact, the CP signal is a limiting case of a more general type of signal, that is, the PP signal [6].

PP signals can be found in many applications such as radar and ionospheric radio. In addition, even though the original transmitted signal is CP, the state of polarization return received by a radar can vary during the observation time. In the last several decades, few literature regarding DOA estimation of PP signals have been addressed. Ko analyzed the reception of PP waves from the standpoint of coherence theory and established its attendant foundations [6]. Subsequently, Ho et al. presented a high-resolution ESPRIT-based method [7] using the electromagnetic vector sensors. Nevertheless, the noncircular properties were not considered. In view of this, Chen proposed a method to take care of the mixed noncircular and circular signals [1] based on MUSIC. Although the MUSIC algorithm has substantial performance advantages, it requires considerable costs in terms of computation and storage for searching over parameter space. Instead, EPSRIT effectively avoids the cumbersome searching process.

In this paper, an extended ESPRIT algorithm is proposed to estimate the DOAs of PP signals. Compared with the existing methods, the proposed one has three main advantages. Firstly, it improves the estimation accuracy by exploiting the polarization information. Secondly, it can still work effectively for scenarios where noncircular and circular signals co-exist. Finally, it does not require pair matching for 2-D DOA estimation which reduces computational burden and extensive search efforts.

The rest of this correspondence is as follows. In Section 2, we show how the extended ESPRIT can be used to estimate the DOAs of PP sources. The Cramer-Rao Lower Bound (CRB) is derived in Section 3. Simulation results for demonstrating the analysis are given in Section 4, followed by concluding remarks.

Received 1 March 2017, Accepted 20 April 2017, Scheduled 2 May 2017

* Corresponding author: Minjie Wu (wmj601@nuaa.edu.cn).

The authors are with the Department of Electronic Science and Engineering, National University of Defense Technology, Deya Street 109, Changsha 410073, China.

2. PROPOSED ALGORITHM

We consider a polarization sensitive array with $N(N = 9)$ elements as shown in Fig. 1. The whole array is composed of N_s $(N_s = 3)$ identical subarrays. Each subarray consists of N/N_s dipoles.We assume that each dipole in the array is a short dipole whose output voltage is proportional to the electric field along the dipole. The first element in each subarray is treated as the reference with respect to other elements, and the corresponding position vectors are $(0, 0, 0)^T$, $(0, dy, dz)^T$ and $(0, dy, -dz)^T$ respectively. In addition, the inter-element spacing between two adjacent dipole is less than the half wavelength to avoid ambiguity problem of angle estimation.

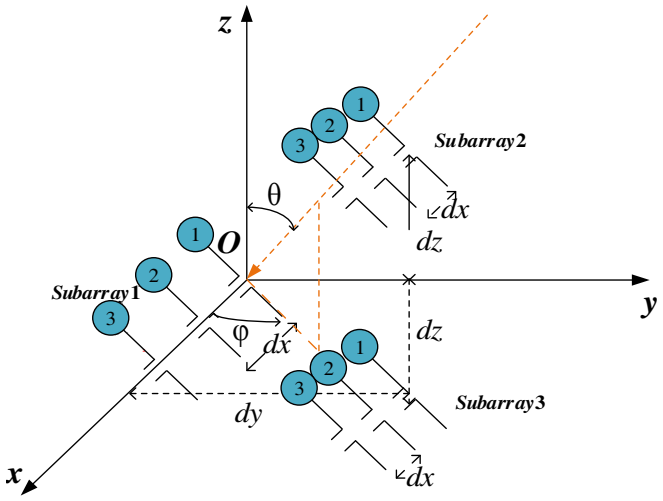

Figure 1. The array geometry.

Assume that there are M far-field narrow band polarization sources. Among them, there are M_1 non-circular signals and M_2 circular signals. θ_m represents the mth signal elevation angle which is measured down from the z axis. φ_m indicates the mth signal azimuth angle, and is measured counterclockwise from the x axis. The arriving signals are assumed to be narrow-band, so the signals received on different subarrays differ only by a phase factor. Let $\mathbf{a}_m^1$ denote the steering vector of Subarray-1 as shown in Fig. 1, then the steering vector of the Subarray-2 and the Subarray-3 are respectively

$$\mathbf{a}_m^2 = \mathbf{a}_m^1 e^{j\frac{2\pi(d_y \sin\theta_m \sin\varphi_m + d_z \cos\theta_m)}{\lambda}} \tag{1}$$

$$\mathbf{a}_m^3 = \mathbf{a}_m^1 e^{j\frac{2\pi(d_y \sin\theta_m \sin\varphi_m - d_z \cos\theta_m)}{\lambda}} \tag{2}$$

where

$$\mathbf{a}_m^1 = \begin{bmatrix} \mathbf{u}_{m,1}^{(9)} & & \\ & \ddots & \\ & & \mathbf{u}_{m,N_s}^{(9)} \end{bmatrix} \mathbf{P}^{(9)} \Theta(\theta_m, \phi_m) \tag{3}$$

with $\mathbf{u}_{m,n}^{(9)} = e^{j\frac{2\pi(n-1)d_x}{\lambda}\sin\theta_m\cos\varphi_m}$ representing the spatial phase factor which relates the mth narrow-band point source to the nth element. $\mathbf{P}^{(9)}$ is the polarization sensitive matrix of the first subarray. In addition, $\Theta(\theta_m, \varphi_m)$ is the steering vector of the angle field and can be expressed as follows

$$\Theta(\theta_m, \varphi_m) = \begin{bmatrix} -\sin\varphi_m & \cos\theta_m\cos\varphi_m \\ \cos\varphi_m & \cos\theta_m\sin\varphi_m \\ 0 & \sin\theta_m \end{bmatrix} = \begin{bmatrix} \mathbf{e}_{hm} & \mathbf{e}_{vm} \end{bmatrix} \tag{4}$$

where $\mathbf{e}_{hm} = [-\sin\varphi_m, \cos\varphi_m, 0]^T$ and $\mathbf{e}_{vm} = [\cos\theta_m\cos\varphi_m, \cos\theta_m\sin\varphi_m, -\sin\theta_m]^T$ represent the horizontal directional vector and the vertical directional vector of the mth signal, respectively.

For arbitrary signals, the data model can be rewritten with the form

$$\mathbf{x}(t) = \mathbf{x}_h(t)\mathbf{e}_h + \mathbf{x}_v(t)\mathbf{e}_v \tag{5}$$

The superscript ^{T} symbolizes the transpose operator.In previous literature, the signals are normally assumed to be CP, viz., $\mathbf{x}_h(t)$ and $\mathbf{x}_v(t)$ are coherent. However, for PP waves, the above two components are uncorrelated. Similarly, we can constitute $\mathbf{a}^1_{hm}$ and $\mathbf{a}^1_{vm}$ be the corresponding steering vectors from $\mathbf{a}^1_m$ in the same way that $\mathbf{x}_h(t)$ and $\mathbf{x}_v(t)$ are formed from $\mathbf{x}(t)$.

Combining (11) and (12), we now have

$$\mathbf{a}^1_{hm} = \begin{bmatrix} \mathbf{u}^{(9)}_{m,1} & & \\ & \ddots & \\ & & \mathbf{u}^{(9)}_{m,N_s} \end{bmatrix} \mathbf{P}^{(9)}\mathbf{e}_{hm} \tag{6}$$

and

$$\mathbf{a}^1_{vm} = \begin{bmatrix} \mathbf{u}^{(9)}_{m,1} & & \\ & \ddots & \\ & & \mathbf{u}^{(9)}_{m,N_s} \end{bmatrix} \mathbf{P}^{(9)}\mathbf{e}_{vm} \tag{7}$$

Then, the output of the array can be expressed in matrix notation

$$\begin{aligned} \mathbf{x}(t) &= \begin{bmatrix} \mathbf{x}_1(t) \\ \mathbf{x}_2(t) \\ \mathbf{x}_3(t) \end{bmatrix} = \begin{bmatrix} \sum_{m=1}^{M} \mathbf{a}^1_m s_m(t) \\ \sum_{m=1}^{M} \mathbf{a}^2_m s_m(t) \\ \sum_{m=1}^{M} \mathbf{a}^3_m s_m(t) \end{bmatrix} + \mathbf{n}(t) \\ &= \begin{bmatrix} \sum_{m=1}^{M} \left[\mathbf{a}^1_{hm} s_{hm}(t) + \mathbf{a}^1_{vm} s_{vm}(t)\right] \\ \sum_{m=1}^{M} e^{j\frac{2\pi(d_y \sin\theta_m \sin\varphi_m + d_z \cos\theta_m)}{\lambda}} \left[\mathbf{a}^1_{hm} s_{hm}(t) + \mathbf{a}^1_{vm} s_{vm}(t)\right] \\ \sum_{m=1}^{M} e^{j\frac{2\pi(d_y \sin\theta_m \sin\varphi_m - d_z \cos\theta_m)}{\lambda}} \left[\mathbf{a}^1_{hm} s_{hm}(t) + \mathbf{a}^1_{vm} s_{vm}(t)\right] \end{bmatrix} + \mathbf{n}(t) \\ &= \begin{bmatrix} \mathbf{A}_1 \\ \mathbf{A}_2 \\ \mathbf{A}_3 \end{bmatrix} \mathbf{s}(t) + \mathbf{n}(t) \end{aligned} \tag{8}$$

where $\mathbf{n}(t)$ denotes the noise vector whose component has a zero mean and a variance which equals to σ^2.

For CP signals, the data model can be written in a similar form, that is

$$\mathbf{x}^c(t) = \begin{bmatrix} \mathbf{x}^c_1(t) \\ \mathbf{x}^c_2(t) \\ \mathbf{x}^c_3(t) \end{bmatrix} = \begin{bmatrix} \sum_{m=1}^{M} \mathbf{a}^{1c}_m s_m(t) \\ \sum_{m=1}^{M} e^{j\frac{2\pi(d_y \sin\theta_m \sin\varphi_m + d_z \cos\theta_m)}{\lambda}} \mathbf{a}^{1c}_m s_m(t) \\ \sum_{m=1}^{M} e^{j\frac{2\pi(d_y \sin\theta_m \sin\varphi_m - d_z \cos\theta_m)}{\lambda}} \mathbf{a}^{1c}_m s_m(t) \end{bmatrix} + \mathbf{n}(t) = \begin{bmatrix} \mathbf{A}^c_1 \\ \mathbf{A}^c_2 \\ \mathbf{A}^c_3 \\ \mathbf{A}^c \end{bmatrix} \mathbf{s}^c(t) + \mathbf{n}(t) \tag{9}$$

where the superscript "c" denotes the CP signal and

$$\mathbf{a}^{1c}_m = \begin{bmatrix} \mathbf{u}^{(1)}_{m,1} & & \\ & \ddots & \\ & & \mathbf{u}^{(1)}_{m,N_s} \end{bmatrix} \mathbf{P}^{(1)}\Theta\left(\theta_m, \phi_m\right)\mathbf{h}\left(\gamma_m, \eta_m\right) \tag{10}$$

with

$$\mathbf{h}\left(\gamma_m, \eta_m\right) = \begin{bmatrix} \cos\gamma_m \\ \sin\gamma_m e^{j\eta_m} \end{bmatrix} \tag{11}$$

Here, the two parameters γ_m and η_m, respectively, denote the polarization auxiliary angle and the polarization phase difference of the mth source.

Let's refer back to Eq. (8), to better demonstrate the rotational invariance relations between subarrays, and let

$$\Gamma_1 = \text{diag}\left[e^{j\varsigma_1}, e^{j\varsigma_1}, \ldots, e^{j\varsigma_M}, e^{j\varsigma_M}\right] \tag{12}$$

$$\Gamma_2 = \text{diag}\left[e^{j\xi_1}, e^{j\xi_1}, \ldots, e^{j\xi_M}, e^{j\xi_M}\right] \tag{13}$$

where

$$\varsigma_i = e^{j\frac{2\pi(d_y \sin\theta_i \sin\phi_i + d_z \cos\theta_i)}{\lambda}} \tag{14}$$

$$\xi_i = e^{j\frac{2\pi(d_y \sin\theta_i \sin\phi_i - d_z \cos\theta_i)}{\lambda}} \tag{15}$$

Then $\mathbf{A}_2 = \mathbf{A}_1\Gamma_1$, $\mathbf{A}_3 = \mathbf{A}_1\Gamma_2$. It follows from Eqs. (8), (12) and (13) that the signal direction cosines are embodied in $\mathbf{A}_1$, Γ_1 and Γ_2. Thus, the DOAs can be estimated through the rotational invariance relationships between subarrays.

The covariance matrix of $\mathbf{x}(t)$ is given by

$$\mathbf{R}_{xx} = E\left\{\mathbf{x}(t)\mathbf{x}^H(t)\right\} = \mathbf{A}\mathbf{R}_{ss}\mathbf{A}^H + \sigma_n^2\mathbf{I}_N = \mathbf{R}_{xx}^H \tag{16}$$

where $\mathbf{I}_N$ is an unit matrix of dimension $N \times N$. $\mathbf{R}_{ss} = E\left\{\mathbf{s}(t)\mathbf{s}^H(t)\right\}$ not only denotes the signal covariance matrix, but also represents the coherency matrix which completely characterizes the state of wave polarization. Additionally, $\mathbf{R}_{ss}$ can be decomposed into the following form

$$\mathbf{R}_{ss} = \frac{\sigma_u^2}{2}\mathbf{I}_2 + \sigma_c^2\mathbf{h}\left(\gamma, \eta\right)\mathbf{h}^H\left(\gamma, \eta\right) \tag{17}$$

where

$$\sigma_c^2 = \sqrt{\left(\mathbf{R}_{ss}\left(1,1\right) - \mathbf{R}_{ss}\left(2,2\right)\right)^2 + 4\mathbf{R}_{ss}\left(1,2\right)\mathbf{R}_{ss}\left(2,1\right)} \tag{18}$$

$$\sigma_u^2 = \mathbf{R}_{ss}\left(1,1\right) + \mathbf{R}_{ss}\left(2,2\right) - \sigma_c^2 \tag{19}$$

It follows from Eq. (17) that a PP signal is composed of a CP signal and a randomly polarized signal. σ_c^2 and σ_u^2 represent the power of CP part and randomly polarized part, respectively.

To proceed further, we will introduce the degree of polarization (p). It is defined as the ratio of the power of the CP component to the total power of the incident wave. Thus, $0 \le p \le 1$. p is independent of the particular choice of the coordinate axes. When p is zero, we may say that the signal is randomly polarized. On the other hand, if p equals unity, the wave is said to be CP. Between these two extreme cases, we have a PP signal. And it shows neither completely regular nor completely irregular variation in the trace of the end point.

The array manifold $\mathbf{A}$ of dimension $N \times 2M$ is always assumed to be full column rank. In addition, let $\mathbf{U}_s$ be the $N \times 2M$ matrix composed of the $2M$ eigenvectors corresponding to the $2M$ largest eigenvalues of $\mathbf{R}_{xx}$. Thus, there exists a unique nonsingular $\mathbf{T}$ with $2M \times 2M$ dimension which relates the $\mathbf{U}_s$ with $\mathbf{A}$, that is

$$\mathbf{U}_s = \mathbf{A}\mathbf{T} \tag{20}$$

Because the subarrays shown in Fig. 1 do not overlap (i.e., share elements), we can get the signal subspace of each subarray

$$\mathbf{U}_{si} = \mathbf{U}_s((i-1)N_s + 1 : iN_s, :) = \mathbf{A}_i\mathbf{T}, \quad i = 1, 2, 3 \tag{21}$$

Then, let

$$\mathbf{U}_{s23} = \mathbf{U}_{s2} + \mathbf{U}_{s3} = \mathbf{A}_1(\mathbf{\Gamma}_1 + \mathbf{\Gamma}_2)T = \mathbf{A}_1\mathbf{\Gamma}_{12}\mathbf{T} \tag{22}$$

$$\mathbf{\Psi} = \mathbf{A}_1\mathbf{\Gamma}_{12}\mathbf{A}_1^+ = \mathbf{A}_1\mathbf{\Gamma}_{12}(\mathbf{A}_1^H\mathbf{A}_1)^{-1}\mathbf{A}_1^H \tag{23}$$

where "+" symbolizes the matrix left inverse and

$$\begin{aligned}\boldsymbol{\Gamma}_{12} &= \boldsymbol{\Gamma}_1 + \boldsymbol{\Gamma}_2 \\ &= \text{diag}\left\{2\cos\left(\frac{2\pi d_z\cos(\theta_1)}{\lambda}\right)e^{j\frac{2\pi d_y\sin\theta_1\sin\varphi_1}{\lambda}}, 2\cos\left(\frac{2\pi d_z\cos(\theta_1)}{\lambda}\right)e^{j\frac{2\pi d_y\sin\theta_1\sin\varphi_1}{\lambda}},\right. \\ &\quad \left.\ldots, 2\cos\left(\frac{2\pi d_z\cos(\theta_M)}{\lambda}\right)e^{j\frac{2\pi d_y\sin\theta_M\sin\varphi_M}{\lambda}}, 2\cos\left(\frac{2\pi d_z\cos(\theta_M)}{\lambda}\right)e^{j\frac{2\pi d_y\sin\theta_M\sin\varphi_M}{\lambda}}\right\} \quad (24)\end{aligned}$$

From Eqs. (21), (22) and (23), the rotational invariance properties between subarrays can be obtained, that is

$$\boldsymbol{\Psi}\mathbf{U}_{s1} = \boldsymbol{\Psi}\mathbf{A}_1\mathbf{T} = \mathbf{A}_1\boldsymbol{\Gamma}_{12}\mathbf{A}_1^{+}\mathbf{A}_1\mathbf{T} = \mathbf{A}_1\boldsymbol{\Gamma}_{12}\mathbf{T} = \mathbf{U}_{s23} \quad (25)$$

We can find $\boldsymbol{\Psi}$ by applying the straightforward approach least-squares (LS). However, under noisy measurements in practical situations, the LS may not be appropriate. Instead, $\boldsymbol{\Psi}$ is often solved by using the total-least-squares (TLS) method. Here, the specific procedure is omitted and the final results are given directly,

$$\boldsymbol{\Psi} = \mathbf{U}_{s23}\mathbf{U}_{s1}^{H}\left(\boldsymbol{\Xi}+\mathbf{U}_{s1}\mathbf{U}_{s1}^{H}\right)^{-1} \quad (26)$$

where $\boldsymbol{\Xi} = \mathbf{I}_{N/N_s} - \mathbf{U}_{s1}\mathbf{U}_{s1}^{+}$.

Multiplying $\mathbf{A}_1$ by (23),

$$\boldsymbol{\Psi}\mathbf{A}_1 = \mathbf{A}_1\boldsymbol{\Gamma}_{12} \quad (27)$$

Then, it is obvious that $2M$ largest eigenvalues of $\boldsymbol{\Psi}$ correspond to the diagonal entries of $\boldsymbol{\Gamma}_{12}$. By calculating the magnitude and the phase of the eigenvalue, we can obtain the corresponding direction cosines along the z axis and the y axis respectively, i.e.,

$$\cos\theta_m = \frac{\lambda\cos^{-1}(|p_m|)}{2\pi d_z} \quad (28)$$

$$\sin\theta_m\sin\varphi_m = \frac{\lambda angle(p_m)}{2\pi d_y} \quad (29)$$

where $|\cdot|$ and $angle(\cdot)$ return the modulus (magnitude) and the phase, respectively. And p_m represents the mth eigenvalue.

In addition, the $2M$ primary eigenvectors of $\boldsymbol{\Psi}$ are proportional to the corresponding $2M$ column vectors of $\mathbf{A}_1$ as long as the diagonal elements are different from each other, a condition that is satisfied in most cases. Then, we have

$$\sin\theta_m\cos\varphi_m = \frac{\lambda angle(v_m(2)/\mathbf{v}_m(1))}{2\pi d_x} \quad (30)$$

Combining Eqs. (29) and (30), the azimuth can be directly given.

$$\tan\varphi_m = \frac{d_x angle(p_m)}{d_y angle(\mathbf{v}_m(2)/\mathbf{v}_m(1))} \quad (31)$$

Note that azimuth and elevation angles are derived based on the corresponding eigenvalues and eigenvectors. Thus, pair matching is not required and the cumbersome search efforts are avoided.

3. DERIVATION OF CRB

In the spatial spectra estimation, CRB [8] is always used to measure the estimation accuracy. From Eq. (3), we know that the unknown variables involve the elevation angle θ_m, the azimuth angle φ_m. In addition, the carrier frequency f_m which embodies in the signal, $\mathbf{s}(t)$, is unknown as well Thus, we define

$$\kappa = \left[\kappa_1^T, \kappa_2^T, \ldots, \kappa_M^T\right]^T \quad (32)$$

where $\kappa_m = [\theta_m, \varphi_m, f_m]^T$. Therefore, $\mathbf{y}(t) \sim N(\boldsymbol{\mu}(\boldsymbol{\kappa}),\ \mathbf{C}(\boldsymbol{\kappa}))$, i.e., a Gaussian vector with mean $\boldsymbol{\mu}(\boldsymbol{\kappa})$ and covariance $\mathbf{C}(\boldsymbol{\kappa})$. In [8], the Fisher information matrix is given by

$$\mathbf{Fim}\left(\kappa\right) = 2\mathrm{Re}\left[\left(\frac{\partial\mu\left(\kappa\right)}{\partial\kappa}\right)^{H}\mathbf{C}^{-1}\left(\kappa\right)\left(\frac{\partial\mu\left(\kappa\right)}{\partial\kappa}\right)\right] = \begin{bmatrix} \mathbf{Fim}_{1,1} & \cdots & \mathbf{Fim}_{1,M} \\ \vdots & \ddots & \vdots \\ \mathbf{Fim}_{M,1} & \cdots & \mathbf{Fim}_{M,M} \end{bmatrix} \tag{33}$$

The $M \times M$ block-matrix form with size 3×3 can be represented as

$$\mathbf{Fim}_{i,j} = \begin{bmatrix} \mathbf{Fim}_{\theta_i,\theta_j} & \mathbf{Fim}_{\theta_i,\varphi_j} & \mathbf{Fim}_{\theta_i,f_j} \\ \mathbf{Fim}_{\varphi_i,\theta_j} & \mathbf{Fim}_{\varphi_i,\varphi_j} & \mathbf{Fim}_{\varphi_i,f_j} \\ \mathbf{Fim}_{f_i,\theta_j} & \mathbf{Fim}_{f_i,\varphi_j} & \mathbf{Fim}_{f_i,f_j} \end{bmatrix} \quad i,j = 1,2,\ldots,M \tag{34}$$

where

$$\mathbf{Fim}_{\kappa_i,\kappa_j} = 2\mathrm{Re}\left[\left(\frac{\partial\boldsymbol{\mu}\left(\kappa\right)}{\partial\kappa_i}\right)^{H}\mathbf{C}^{-1}\left(\kappa\right)\left(\frac{\partial\boldsymbol{\mu}\left(\kappa\right)}{\partial\kappa_j}\right)\right] \tag{35}$$

Moreover, it is worthwhile to note that $\mathbf{Fim}_{\kappa_j,\kappa_i}$ equals $\mathbf{Fim}_{\kappa_i,\kappa_j}$. Thus, $\mathbf{Fim}_{i,j}$ is symmetric which decreases the computational burden by half. For CRB is found as the $(i,\ j)$th element of the inverse of $\mathbf{Fim}$. Thus, CRB can be obtained.

4. SIMULATION RESULTS

In this section, Monte-Carlo simulation experiments are used to verify the effectiveness of the P-ESPRIT algorithm. The array structure is shown in Fig. 1. Among which, we select N and N_s as 9 and 3 respectively. Thus, each subarray contains 3 dipoles. The root mean squared error (RMSE) is utilized as the performance measure and 200 independent simulation experiments are carried out. The RMSE is defined as

$$RMSE = \sqrt{\frac{1}{200}\sum_{i=1}^{200}\left[\left(\hat{\theta}_i - \theta_i\right)^2 + \left(\hat{\varphi}_i - \varphi_i\right)^2\right]} \tag{36}$$

where $\left\{\hat{\theta}_i, \hat{\varphi}_i\right\}$ are the estimates of elevation angles and azimuth angles, respectively, at the ith run. In addition, Li's method [9] and Tayem's method [10] are included for comparison.

Provided that one BPSK (noncircular) signal and one QPSK (circular) signal can be received, the incident angles are respectively (50°, 35°), (70°, 65°). The snapshot, K, is selected as 200. The signal-to-noise (SNR) used in the simulations is 20 dB.

Figure 2 displays the simulation results of estimating the DOA of BPSK and QPSK signals using P-ESPRIT algorithm. Intuitively, the estimation accuracy is high and the peaks appear around (50°, 70°), (35°, 65°). It is worthwhile to note that the estimation accuracy of the BPSK single is close to that of the QPSK signal. The reason is that the data model in Eq. (8) does not exploit the noncircular properties. To proceed further, we can use Eq. (8) to construct the conjugate augmented output vector by combining the observed signal vector and its complex conjugate counterpart.

$$\mathbf{x}_1^h(t) = \sum_{m=1}^{M}\begin{bmatrix} \mathbf{a}_{hm}^1 \\ e^{-j\varpi_m^h}\mathbf{a}_{hm}^{1*} \end{bmatrix} s_{hm}(t) = \mathbf{A}_{1h}\mathbf{s}_1^h(t) \tag{37}$$

$$\mathbf{x}_1^v(t) = \sum_{m=1}^{M}\begin{bmatrix} \mathbf{a}_{vm}^1 \\ e^{-j\varpi_m^v}\mathbf{a}_{vm}^{1*} \end{bmatrix} s_{vm}(t) = \mathbf{A}_{1v}\mathbf{s}_1^v(t) \tag{38}$$

where ϖ_m^h and ϖ_m^v stand for the horizontal and vertical components of the mth signal noncircular phase, respectively. $\mathbf{x}_2^h(t)$ and $\mathbf{x}_3^h(t)$ can be obtained in the same way. Then, the noncircular properties are embodied in the data model. Keep other experimental conditions unchanged, the corresponding simulation results is shown in Fig. 3. Compared with Fig. 2, it is obvious that the accuracy of the BPSK signal is improved by exploiting the noncircular properties.

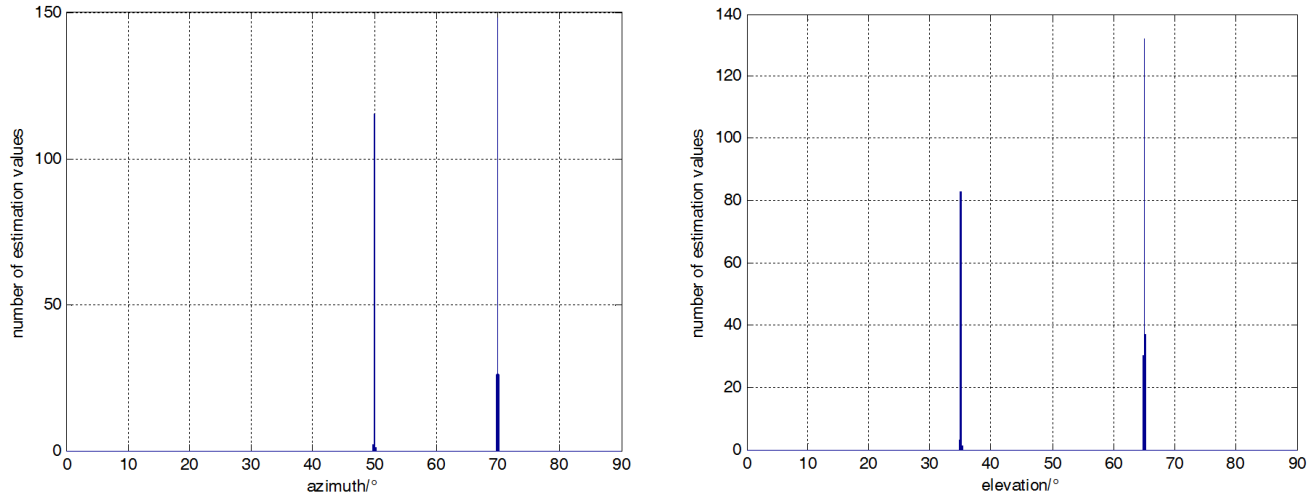

Figure 2. Histogram of DOA Estimations (a) azimuth (b) elevation.

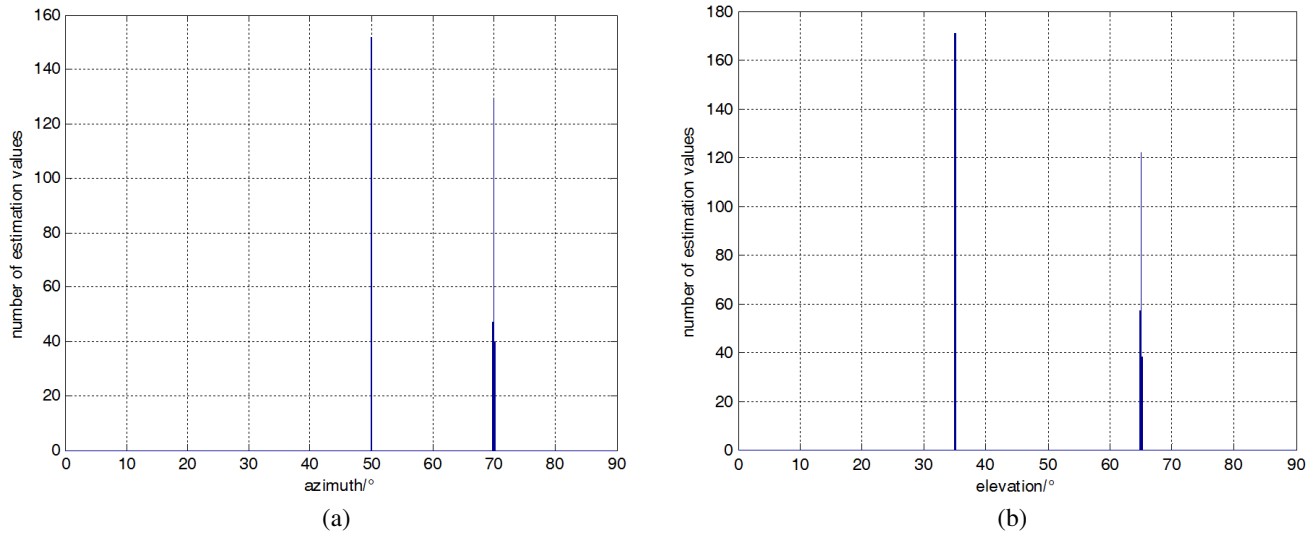

Figure 3. Histogram of DOA Estimations using noncircularity (a) azimuth (b) elevation.

Figure 4 shows that the CRB for multiple parameters estimation of the first source (T1). Fig. 4(a) displays the CRB versus SNRs with snapshots being 200 while Fig. 4(b) describes the relationship between CRBs and the number of snapshots with SNR fixed at 20 dB. It is not hard to conclude that the CRB of all parameters decline with the increase of SNR and the number of snapshots. In particular, we use the curve of elevation as an analytical model and pick the points with snapshots being 400 and 800 respectively, we may find that the corresponding variances of CRB are -64.95 dB and -67.96 dB. This means that the former value is nearly twice as much as the latter one. In fact, these improvements can be predicted from the derivation of CRB. The specific derivation process can refer to the literature [8]. The number of snapshots can be extracted from the Fisher information matrix. Moreover, the CRB is found as the element of the inverse of that matrix. So, we can conclude that CRB is inversely proportional to K. Thus, the estimation precision will be higher.

In addition, since all the information is embodied in the observed data and the underlying probability distribution function (PDF) for that data, it is not surprising that the estimation accuracy

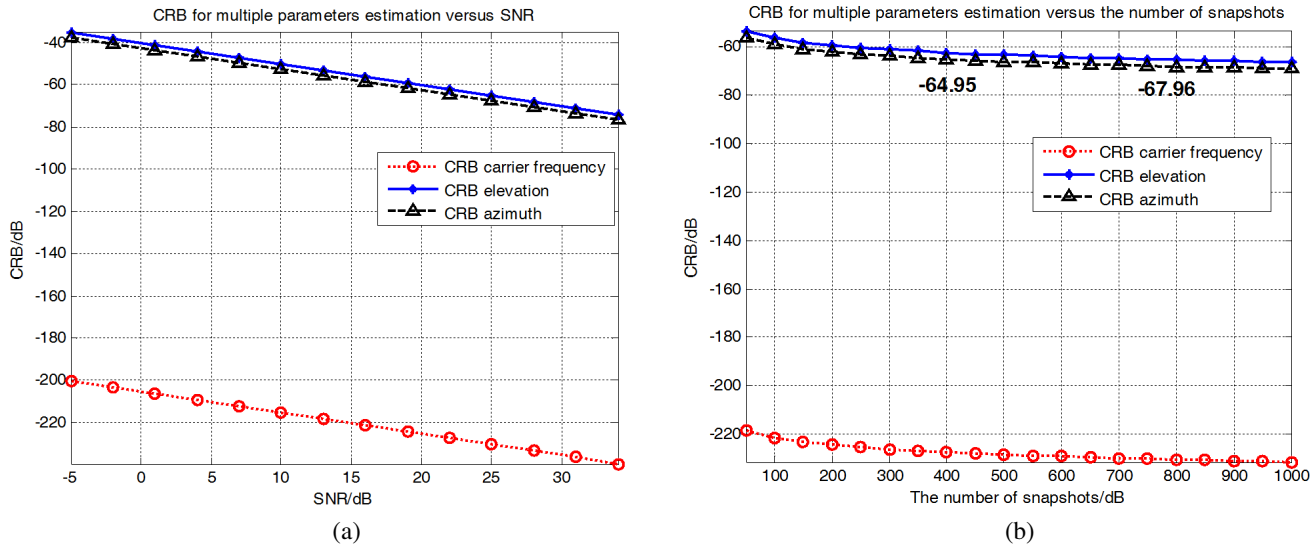

Figure 4. CRB for multiple parameters estimation of the first source (a) CRB versus snapshots with SNR fixed at 20 dB (b) CRB versus SNRs with snapshots being 200.

depends directly on the PDF. In general, the more the PDF is influenced by the unknown parameter, the better the estimation accuracy is. From these two figures, we find that the variance of the CRB for carrier frequency is lower than the CRB for other parameters. These different dependences indicate that CRB is more sensitive to changes in carrier frequency than to changes in other parameters. Thus, we can infer that the PDF is more sensitive to the carrier frequency than other parameters.

In Section 3, we assume that there are three unknown parameters. However, in this correspondence, the estimation accuracies of azimuth and elevation are focuses. Thus, in order to analyze the performance of the extended ESPRIR quantitatively, we plot the CRB versus azimuth and elevation. Then, the Fisher Information Matrix can be further simplified. Rewrite Eq. (34)

$$\mathbf{Fim}_{i,j} = \begin{bmatrix} \mathbf{Fim}_{\theta_i,\theta_j} & \mathbf{Fim}_{\theta_i,\varphi_j} \\ \mathbf{Fim}_{\varphi_i,\theta_j} & \mathbf{Fim}_{\varphi_i,\varphi_j} \end{bmatrix}; \quad i,j = 1,2,\ldots,M \tag{39}$$

The corresponding simulation results are given in Fig. 5. The SNR is 20 dB, and the number of snapshots equals 200. We find that the estimation accuracies vary with the locations of the source. In some regions, the estimation accuracies are seriously deteriorated. When the DOAs become larger, the estimation accuracies get worse. The reason is that when the signal is far away from the normal direction of the array, the actual aperture of the array is reduced along the direction of signals. As a matter of fact, compared with Eq. (34), the simulation results using Eq. (39) are improved over the entire range. This is a quite general result that asserts that the CRB always increases as we estimate more parameters. The detailed analysis is presented in [8], which is beyond the scope of this paper.

Figure 6 shows the improvements of the proposed algorithm over existing ones, such as Tayem's C-SPRIT [10] and Li's method [9]. We study the performance with a varying SNR from 0 dB to 30 dB. Without loss of generality, we select the first source (T1) and the second source (T2), respectively, to verify it. As shown in Fig. 6, the proposed method outperforms the other two methods by exploiting the polarization information of the received data. In [10], the paper claims the conjugate ESPRIT can estimate the DOAs of BPSK signals. However, the noncircular properties are not considered and the polarization information is not reflected in the corresponding simulation results. In addition, it is worthwhile noting that the elevation is given directly in [10] whereas the azimuth is not. And the accumulative errors are inevitably incurred. To remove these problems, the proposed algorithm combines Eqs. (29) and (30), and the azimuth and elevation angles are directly given based on the eigenvalues and the corresponding eigenvectors. Thus, the accumulative errors are effectively averted which results in the higher estimation accuracy.

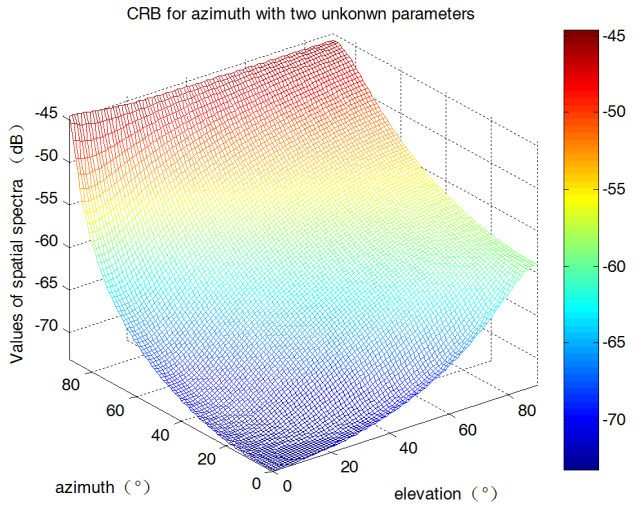

Figure 5. CRB versus azimuth and elevation.

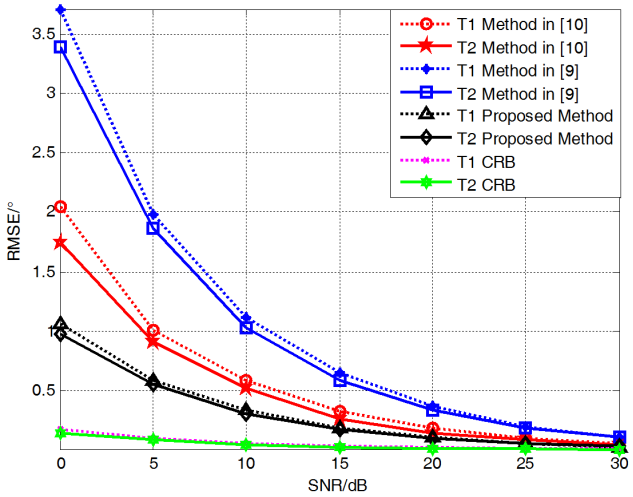

Figure 6. Improvements of the proposed method.

5. CONCLUSION

In this paper, a novel algorithm is proposed to deal with the PP signals. And it effectively estimates the DOAs of mixed noncircular and circular signals. Compared with the existing methods, the proposed one has three main advantages. Firstly, it improves the estimation accuracy by exploiting the polarization information. Secondly, it can still work effectively for scenarios where noncircular and circular signals coexist. Finally, it does not require pair matching for 2-D DOA estimation which reduces computational burden and extensive search efforts. The simulation results also verify the efficacy of the presented method.

ACKNOWLEDGMENT

This project was supported by the National Natural Science Foundation of China (Grant No. 61302017).

REFERENCES

1. Chen, H., C.-P. Hou, W. Liu, W.-P. Zhu, and M. N. S. Swamy, "Efficient two-dimensional direction-of-arrival estimation for a mixture of circular and noncircular sources," *IEEE Sensors Journal*, Vol. 16, 2527–2536, Apr. 2016.
2. Gao, F.-F., A. Nallanathan, and Y.-D. Wang, "Improved MUSIC under the coexistence of both circular and noncircular sources," *IEEE Transactions on Signal Processing*, Vol. 56, No. 7, 3033–3038, Jul. 2008.
3. Wu, M.-J., X.-F. Zhang, J.-J. Huang, and N.-C. Yuan, "DOA estimation of cylindrical conformal array based on geometric algebra," *International Journal of Antennas and Propagation*, 2016, Available: http://dx.doi.org/10.1155/2016/7832475.
4. Liu, J., Z.-T. Huang, and Y.-Y. Zhou, "Extend 2q-MUSIC algorithm for noncircular signals," *Signal Processing*, Vol. 88, 1327–1339, Dec. 2008.
5. Nie, W.-K., D.-Z. Feng, H. Xie, J. Li, and P.-F. Xu, "Improved MUSIC algorithm for high resolution angle estimation," *Signal Processing*, Vol. 122, 87–92, Dec. 2015.
6. Ko, H. C., "On the reception of quasi-monochromatic, partially polarized radio waves," *Proceedings of the IRE*, Vol. 50, No. 9, 1950–1957, 1962.

7. Ho, K.-C., K.-C Tan, and B. T. G. Tan, "Efficient method for estimating directions-of-arrival of partially polarized signals with electromagnetic vector sensors," *IEEE Transactions on Signal Processing*, Vol. 45, No. 10, 2485–2498, Oct. 1997.
8. Kay, S. M., *Fundamentals of Statistical Signal Processing Volume I: Estimation Theory*, Pearson Education, Inc., USA, ISBN: 978-0133457117, 1993.
9. Li, J., X. Zhang, and H. Chen, "Improved two-dimensional DOA estimation algorithm for two-parallel uniform linear arrays using propagator method," *Signal Processing*, Vol. 92, 3032–3038, 2012, DOI: 10.1016/j.sigpro.2012.06.010.
10. Tayem, N. and H. M. Kwon, Conjugate ESPRIT (C-SPRIT), *IEEE Transactions on Antennas and Propagation*, Vol. 52, No. 10, 2618–2624, 2004, ISSN: 0018-926X. DOI: 10.1109/TAP.2004.834385.